International Journal of Thermal Sciences 49 (2010) 522–528

Contents lists available at ScienceDirect

International Journal of Thermal Sciences

journal homepage: www.elsevier.com/locate/ijts

Modelling the nucleation process in alumina lamellae deposited on a steel substrate

Y. Lahmar-Mebdoua [a,*], A. Vardelle [b], P. Fauchais [b], D. Gobin [c]

[a] Centre de Développement des Technologies Avancées, Baba Hassen, Algiers, Algeria
[b] Laboratoire Science des Procédés Céramiques et de Traitements de Surface UMR-CNRS 6638, University of Limoges, France
[c] Laboratoire FAST, Univ. Pierre et Marie Curie, CNRS, F-91405 Orsay, France

ARTICLE INFO

Article history:
Received 13 June 2009
Received in revised form
21 September 2009
Accepted 28 September 2009
Available online 30 September 2009

Keywords:
Plasma spraying
Splat formation
Numerical modelling
Heat transfer
Nucleation
Rapid solidification
Thermal contact resistance

ABSTRACT

A one-dimensional model has been developed to address the non-equilibrium heat transfer between an alumina lamella deposited by plasma spraying, and a steel or alumina substrate. The model includes under-cooling phenomenon, heterogeneous nucleation and crystal growth kinetics, allowing for the prediction of the temperature evolution in the lamella and substrate and of the nucleation temperature, grain density and size distribution. The effect on the nucleation process of the contact angle between the nucleus and substrate surface and of the quality of the contact at the splat–substrate interface is emphasized. The influence of the splat thickness, substrate material and substrate oxidation on the grain size distribution is also discussed.

1. Introduction

A plasma-sprayed coating consists of layered individual splats, each one being formed by the impingement of molten or semi-molten particles on a solid substrate. Each liquid particle flattens forming a splat that cools down and solidifies, solidification often starting before flattening is completed. The microstructure of such coatings and their properties are strongly linked: (i) to the morphology of the splats and (ii) to the quality of the contacts between splats and substrate and between splats [1]. On a smooth substrate the splat shape depends on parameters related to the impacting particles (size, velocity, temperature, molten state, material nature and oxidation stage) and to the substrate (nature, roughness, oxidation stage, temperature) and also on parameters concerning the interface between splats and substrate or previously deposited layers (quality of the contact, wettability, impact pressure).

On smooth substrates, it has been widely observed [1–3] that the splat shape varies from a distorted shape to a lenticular shape. For given impact conditions, this shape transition occurs when the substrate temperature reaches a so-called "transition temperature" T_t.

This drastic change in the splat morphology has been extensively studied both experimentally and numerically [4–8]. The first numerical simulations of droplet impact on a solid smooth surface under plasma spray conditions were carried out assuming a two-dimensional geometry with perfect contact between the splat and substrate [9–11]. Bussmann et al. [12,13] have developed a 3D numerical model of free-surface flow based on the extension of the 2D RIPPLE algorithm to 3D [14]. However, this model did not take into account the heat transfer to the substrate and ambient gas. Passandideh-Fard et al. [15] extended the above model by including heat transfer and solidification, occurring at melting temperature. The temperature discontinuity at the droplet/substrate contact was modelled by a constant thermal contact resistance R_{th}, varying from 10^{-6} to 10^{-7} m^2 K/W. They showed, for example, that the onset of solidification at the beginning of droplet flattening had a drastic effect on the final splat shape and that delaying splat solidification, under certain conditions, suppressed the splashing mechanism.

Jiang et al. [16] explained the transition in splat morphology at the transition temperature, by the desorption of the condensates and adsorbates present at the substrate surface. At room temperature, the latter trapped under the impacting droplet vaporized, impeding the contact between the spreading material and substrate. When the substrate temperature increases, the adsorbed matter evaporates resulting in a cleaner substrate surface and the

* Corresponding author.
E-mail address: yamina.lahmar@gmail.com (Y. Lahmar-Mebdoua).

1290-0729/$ – see front matter © 2009 Elsevier Masson SAS. All rights reserved.
doi:10.1016/j.ijthermalsci.2009.09.011

better contact between the flattening particle and substrate brings about disk-shaped splats. Fukumoto et al. and Cedelle et al. [3,6] showed that preheating the substrate could also modify the liquid/substrate wettability, producing nano-scale oxide peaks on stainless steel substrates. This change in the surface topography improved the quality of contact at the splat–substrate interface and also resulted in disk-shaped splats. The surface is then characterized by a skewness parameter $S_k > 0$, which measures the asymmetry of the surface deviations about the mean plane. This parameter is defined as [6]:

$$S_k = \frac{1}{\sigma^3} \int_{-\infty}^{+\infty} (z-m)^3 \phi(z) \mathrm{d}z \quad (1)$$

where z is the surface height, m its mean value, $\phi(z)$ is the distribution function of the surface heights and σ is the standard deviation of the surface heights.

In fact, preheating metallic substrates promotes the growth of a superficial oxide layer whose composition and thickness condition splat shape and coating adhesion [17]. Bianchi et al. [18] have shown that ceramic coatings obtained on stainless steel substrate preheated at 573 K exhibit an excellent adhesion; the latter decreasing when the oxide layer thickness exceeds 50 nm. With low carbon steel substrate, it has been shown that alumina splats deposited on $Fe_{1x}O$ have an excellent adhesion which deceases as the oxide layer composition changes to Fe_3O_4 and becomes poor on Fe_2O_3 [17]. Pêch [19] observed also the formation of an oxide layer composed of Fe_2O_3 and Fe_3O_4 whose thickness is about 500 nm on a preheated low carbon steel substrate.

Recently, Dhiman et al. [8] proposed a prediction of the splat morphology based on a unique parameter, called the solidification parameter (Θ). This parameter was defined as the ratio of the thickness of the solid layer that appeared in the spreading and solidifying liquid and the splat thickness. In their analysis, the authors took into account important parameters such as the substrate temperature, the thermal contact resistance, the thermo-physical properties of splat and substrate materials and the impact Reynolds and Weber numbers. The dimensionless parameter (Θ), varying between 0 and 1, was analytically calculated using a one-dimensional heat conduction model of splat solidification, where substrate temperature and thermo-physical properties of splat and substrate materials were taken into account. The authors showed that the splat exhibited a fragmented morphology when the parameter Θ was either ($\Theta << 1$) or ($\Theta > 0.4$). In the first case, the solidification process was negligible during spreading; the particle spread into a thin layer and then got fragmented. In the second case, solidification was very rapid, inducing the formation of a solid ring around the edge of the spreading droplet that obstructed liquid spreading and resulted in a fragmented or retracted splat. When the parameter Θ ranged between 0.1 and 0.4, the solid layer formed during droplet spreading retained the liquid from rupture leading to disk-shaped splat.

However, to the best of authors' knowledge, all these models assume that splat solidification occurs at the melting temperature. To describe non-equilibrium phenomena, only one-dimensional heat transfer models of the liquid–solid transformation (liquid under-cooling, nucleation and crystal growth kinetics) are used. Such models are based on the solution of the heat transfer equation in the substrate and the solidifying splat. Generally, a heat transfer coefficient h is introduced at the splat–substrate interface, linked to the thermal contact resistance ($R_{\mathrm{th}} = 1/h$) which models the quality of the surface between the splat and the substrate. The h coefficient may vary from 10^6 to 10^8 W/m^2 K [20–23]. These models consider heterogeneous nucleation where the critical energy strongly depends on the contact angle (β) between the nucleus and substrate surface. The interface temperature is correlated to the interface velocity through a linear kinetic equation [23]. The predictions obtained with these models show that the liquid material could reach a significant under-cooling degree [22,24].

The work presented in this paper deals with a one-dimensional heat transfer model between plasma-sprayed alumina splats and smooth steel and alumina substrates. Indeed, if the first alumina droplets impact on steel, the following droplets impact on a layer of re-solidified alumina lamellae. The model takes into account melt under-cooling, heterogeneous nucleation at the splat–substrate interface and crystal growth. Compared to previous works, the presence of the oxide layer on the preheated metallic substrates is taken into account and the effect of this oxidation on the nucleation process is investigated.

Alumina was selected for this study because its thermal and physical properties are well known and also because it is used as protective or functional coatings. Its interesting service properties (high-temperature creep resistance, high melting temperature, good wear resistance, hardness and good electrical resistivity) are used for many applications in mechanical, refractory, medical, electric, electronic and optical industries [25].

This paper investigates the effect of various parameters on the nucleation process of individual splats: thermal contact resistance at the splat/substrate interface, contact angle between the nucleus and the substrate, splat thickness, substrate temperature and substrate oxidation stage. First the mathematical model is presented with its assumptions, then the predictions obtained for alumina splats on steel and alumina substrates are discussed. Comparisons between predictions and experimental data conclude the study.

2. Mathematical model

2.1. Assumptions

The model developed in this study is based on the following assumptions:

- droplet spreading and solidification processes are considered as two independent phenomena and the model only deals with the thermal problem,
- the model is mono-dimensional: the thickness of the splat (1–2 μm) is small compared to its diameter (30–100 μm) and heat flux is assumed to be in the normal direction to the substrate surface, so that the solidification front is planar and parallel to this surface,
- the thermal properties of the splat and substrate materials are constant, but different for the liquid and solid phases,
- the model includes melt under-cooling, heterogeneous nucleation and crystal growth kinetics, assuming that nucleation starts at the substrate surface,
- the substrate remains solid during the splat cooling process.

2.2. Basic equations

The model is based on the time-dependent heat equation in the solidifying splat and in the substrate.

$$\frac{\partial T_i}{\partial t} = \alpha_i \frac{\partial^2 T_i}{\partial x^2} \quad (2)$$

where α is the thermal diffusivity and the subscript i denotes either the solid part of the splat ($i = s$, $0 > x < s^*$), its liquid part ($i = \mathrm{l}$, $s^* < x < L$), or the substrate ($i = T$, $x < l_{\mathrm{T}} < 0$).

At $t = 0$, the liquid splat with a uniform temperature $T_l > T_m$ (melting temperature) is deposited on the substrate at an initial temperature $T_0 < T_m$. Then, the liquid cools down until the onset of nucleation is followed by solidification.

2.2.1. Boundary conditions

- the heat losses at the top surface of the splat are calculated using the Newton's law of cooling with a heat transfer coefficient, h, which includes convection and linearized radiation. Its value is set at 100 W/m^2 K [22]:

$$-k_L\frac{\partial T_l}{\partial x}\Big)_L = h(T_L(L) - T_{ext}) \tag{3}$$

where L is the splat thickness and T_{ext} the temperature of the surrounding atmosphere.

- a zero heat flux condition is assumed at the bottom l_T of the substrate:

$$k_T\left(\frac{\partial T_T}{\partial x}\right)_{-l_T} = 0 \tag{4}$$

- the contact at the splat–substrate interface is modelled by a thermal contact resistance R_{th}:

$$k_s\frac{\partial T_s}{\partial x}\Big)_{0^+} = -k_T\frac{\partial T_T}{\partial x}\Big)_{0^-} = \frac{T_T(0^-) - T_s(0^+)}{R_{th}} \tag{5}$$

- At the moving solid–liquid interface $s^*(t)$, the heat balance equation yields the Stefan condition:

$$k_s\frac{\partial T_s}{\partial x}\Big)_{s^*} - k_l\frac{\partial T_l}{\partial x}\Big)_{s^*} = \rho_l\Delta H_m v_i \tag{6}$$

where ρ is the density, ΔH_m is the heat of fusion and v_i is the interface solidification velocity. In order to take into account the kinetics effect of the non-equilibrium solidification, the Stefan equation is coupled to the linear kinetics growth equation [23]:

$$v_i = K_M(T_m - T_{int}) \tag{7}$$

where $(T_m - T_{int}) = \Delta T$ represents the under-cooling degree.

The onset of nucleation is calculated from the nucleation rate according to the classical theory of nucleation [26]; the liquid temperature at this instant is assumed to correspond to the nucleation temperature T_N.

The nuclei formation rate depends on a critical free energy change ΔG_c above which the nucleus grows by attachment of the surrounding atoms:

$$\Delta G_c = \frac{16\pi T_m^2\gamma^3 f(\beta)}{3\rho_l^2\Delta H_m^2\Delta T^2} \tag{8}$$

where $f(\beta)$ represents the role of the contact angle β in lowering the energy barrier of nucleation:

$$f(\beta) = \frac{(2 - 3\cos(\beta) + \cos^3(\beta))}{4} \tag{9}$$

More details on the nucleation model are given elsewhere [25,27].

In this study, three alumina phases were considered: the stable phase α and two metastable phases, δ and γ. The phase of the first nucleus corresponds to the selected phase among the three phases in competition. The latent heat released by the growing nuclei constitutes the heat source term affecting the heat balance in the liquid splat expressed as:

$$q = \rho_s\cdot\Delta H_m\cdot\frac{\partial V}{\partial t} \tag{10}$$

where $\partial V/\partial t$ is the rate of volume variation of all the growing grains and ρ_s the solid phase density.

2.3. Numerical method

The Landau front immobilization technique [28] is used to compute the moving solid–liquid interface in the splat on a fixed numerical domain. The transformed equations are discretized using a finite volume technique [29] with a second order implicit spatial scheme leading to a system of linear equations. The non-linear nature of the problem lies in the fact that the matrix coefficients are dependent on the solution itself (position and velocity of the solidification front) which leads to use an iterative procedure. More details on the numerical method are given elsewhere [22,27].

3. Parameters controlling nucleation

As mentioned above, the nucleation kinetics depends on the energy barrier ΔG_c, which is a function of the liquid under-cooling degree ΔT, of the interfacial solid–liquid energy γ_{ls}, of the latent heat of fusion of the material, of the nature of material and of the contact angle between the nucleus and substrate surface (β). In the case of heterogeneous nucleation, the nucleus has a spherical cap shape, and nucleation stops when grains cover 67% of the splat surface in contact with the substrate, corresponding to the portion of a disk surface covered by close-packed circles. The grain number per unit surface (1 m^2) corresponds to the grain density.

The study investigates the effects on the nucleation process of the splat thickness, substrate nature, thickness of the oxide layer formed on the preheated surface of the steel substrate, contact angle β and thermal contact resistance R_{th} between splat and substrate.

The thickness of the splat in this study corresponds to the experimental observations [30]; they are presented in Table 1 for 35-μm diameter plasma-sprayed alumina particles with the corresponding flattening degree.

Table 2 summarizes the other splat and substrate parameters used in the calculations.

The thermal contact resistances were drawn from the experimental data obtained by Bianchi et al. [4]: 10^{-8}–10^{-7} m^2 K/W represents a good splat–substrate contact (substrate preheated at a temperature above the transition temperature: $T_t = 573$ K) whereas 10^{-6} m^2 K/W is related to a bad contact with a substrate whose initial temperature (323 K) is below the transition temperature, T_t.

According to Pêch [19], the preheating of low carbon steel substrates induces the growth of an oxide layer consisting of Fe_2O_3 and Fe_3O_4 with a thickness of about 500 nm whereas the thickness of the spinel formed on the 304 L stainless steel preheated substrate is negligible (up to 50 nm).

3.1. Effect of the contact angle β

The contact angle β may range from 0° to 180°:0° corresponds to perfect wetting of the substrate with no energy barrier for

Table 1
Splat thickness and corresponding flattening degree and surface area.

Splat thickness L (μm)	0.8	1	1.5	2	3	4
Flattening degree $\zeta = D/d$	5.4	4.8	3.9	3.4	2.7	2.4
Splat surface area (μm^2)	9025	7225	4761	3600	2401	1764

Table 2
Input parameters for splat and substrate.

Splat material	Substrate	T_0 (K)	Thermal contact resistance, R_{th} (m^2 K/W)	Oxide layer thickness (nm)	Contact angle β (°)
Alumina	Stainless	573	10^{-7} and 10^{-8}	40	0–90
$T_l = 2800$ K	steel AISI 304 L	323	10^{-6}	20[a]	
	Steel XC38	573	10^{-7} and 10^{-8}	500	
		323	10^{-6}	40[a]	
	γ-Alumina	573	10^{-7} and 10^{-8}	–	
		323	10^{-6}	–	

[a] Oxide layer thicknesses formed on smooth and cold metallic substrate.

nucleation and 180° ($f(\beta) = 1$) corresponds to the case of homogeneous nucleation. As the evolution of $f(\beta)$ is symmetric with respect to $\beta = 90°$, the variation of β has been limited between 0° and 90° and the calculations of the nucleation temperature and grain density were performed for various contact angles between 0° and 90°. The predictions are presented in Figs. 1 and 2. According to [7] increasing the contact angle brings about an increase in the energy barrier ΔG_c and therefore a decrease in the nucleation rate. The calculations confirm the selection of the γ phase which is the most frequently observed phase in plasma-sprayed coatings for $\beta > 55°$. Actually at a lower contact angle ($\beta < 35°$) the liquid perfectly wets the substrate, which corresponds to a decrease of the energy barrier and to the nucleation of the stable α-phase as shown in Fig. 1. Fig. 2 shows that the nucleation temperature T_N strongly depends on the contact angle, because the barrier energy for nucleation is also a function of the under-cooling degree [7] that varies from about 10 K for $\beta = 10°$–580 K for 90°.

Fig. 1 also shows the effect of the quality of the contact at the splat–substrate interface on the grain density. The latter is higher when the thermal contact resistance R_{th} is the lower (10^{-8} m^2 K/W). Indeed, the improvement of the thermal contact results in an increase of the effective contact surface at the splat–substrate interface and thus of the number of atoms or molecules available for nucleation. Whereas the nucleation temperature is not significantly affected by the thermal contact resistance, as shown in Fig. 2, a slight decrease in T_N is observed at lower thermal contact resistance, this change becoming visible for $\beta > 60°$.

Fig. 3 shows that the nucleation temperature does not depend on the splat thickness. Actually the nucleation is a thermally-activated process which depends on the contact angle, splat material and under-cooling degree.

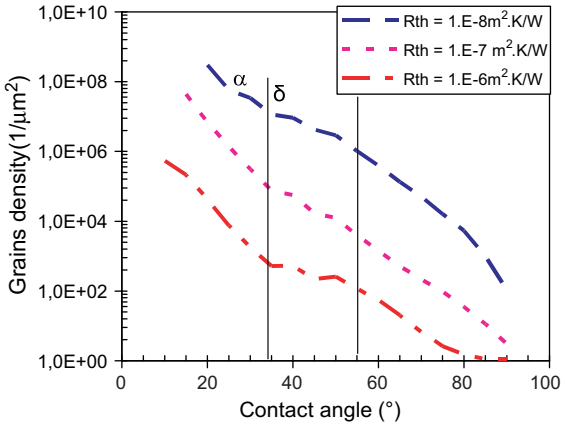

Fig. 1. Effect of the contact angle and of the thermal contact on the grain density for a 1-µm thick alumina splat deposited on stainless steel substrate.

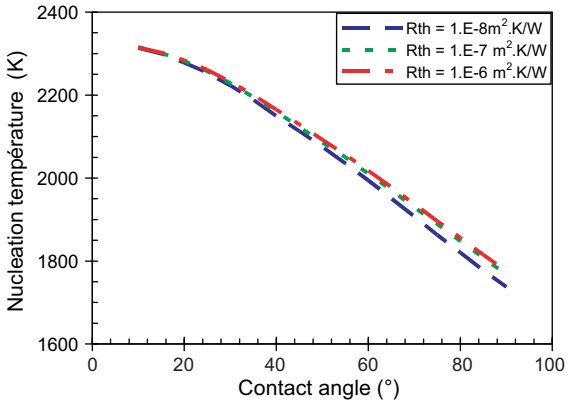

Fig. 2. Effect of the contact angle and of the thermal contact on the nucleation temperature for a 1-µm thick alumina splat deposited on stainless steel substrate.

3.2. Grain size distribution

As the γ-Al_2O_3 phase is the most frequently obtained in actual coatings, and as it corresponds to $\beta > 60°$, the value $\beta = 70°$ has been used in calculations. The model predicts the size distribution of the grains formed during the nucleation process. In the case of alumina material, the melt under-cooling leads to heterogeneous nucleation of γ-Al_2O_3 whose under-cooling degree $\Delta T > 0.14T_m$ which is responsible of the columnar growth occurring in plasma-sprayed coatings [31].

3.2.1. Effect of splat thickness

The under-cooling degree is controlled by the capacity of the splat to release the heat from the melt and that released during crystallization to the substrate; the process depends on the splat thickness. Fig. 4 shows the grain size distribution for alumina splat with different thickness deposited on 304 L stainless steel substrate. The grain size distribution is shifted to higher mean values as the splat thickness increases. As expected, the heat extraction rate is more efficient for thin splats than for thicker ones. The mean grain radius is on the order of 62 nm for 1-µm thick alumina splats and 80 nm for 4-µm thick splats.

3.2.2. Effect of the substrate material

In order to investigate the effect of the thermal properties of the substrate material on the nucleation and solidification processes,

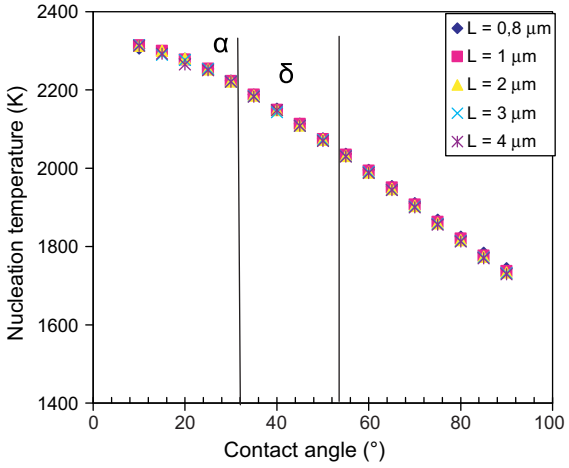

Fig. 3. Variation of nucleation temperature with contact angle for different splat thickness, $R_{th} = 10^{-8}$ m^2 K/W.

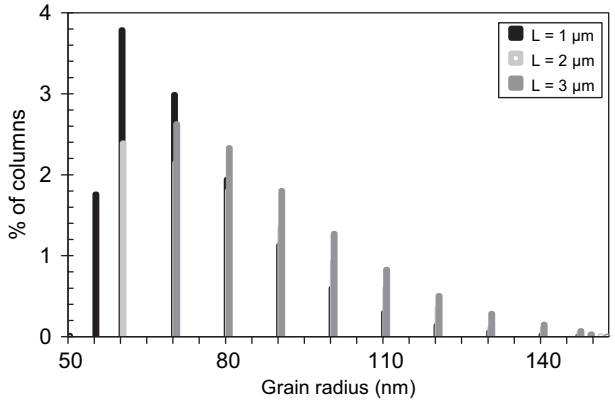

Fig. 4. Effect of splat thickness on the grain size distribution for alumina splats deposited on 316 L stainless steel substrate, $R_{th} = 10^{-7}$ m^2 K/W, $\beta = 70°$.

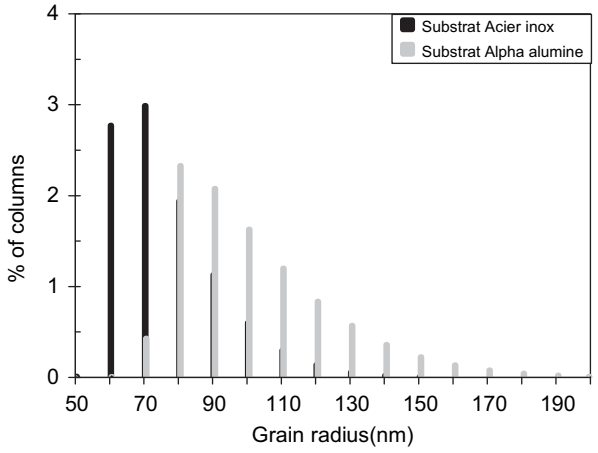

Fig. 6. Effect of substrate material on grain size distribution, 1-µm thick splat, $R_{th} = 10^{-7}$ m^2 K/W.

computations have been performed with two different substrates: stainless steel 304 L and γ-Al_2O_3. The latter also models the deposition of the splat on already-solidified layers. The thermal conductivity and diffusivity of γ-alumina are 5 W/m K and 10^{-6} m^2/s, respectively, while those of stainless steel are 6 W/m K and $4 \cdot 10^{-6}$ m^2/s [25]. This difference results in a slower cooling of the splat on γ-alumina substrate. Fig. 5 shows that the surface of the stainless steel substrate under the splat reaches a temperature of about 1100 K while that of γ-alumina substrate increases up to 1400 K. The thermal properties of substrate affect the grain size distribution as shown in Fig. 6: the size of grain is larger on γ-alumina substrate.

3.2.3. Effect of thermal contact resistance

The quality of the contact at the splat/substrate interface is expressed through the thermal contact resistance R_{th}. A value of R_{th} of 10^{-8} m^2 K/W corresponds to a nearly perfect contact; it can be achieved when the substrate is preheated at temperature $T_0 > T_t$ that makes it possible to desorb the condensates and adsorbates present at the substrate surface. The efficient heat extraction from the splat brings about a fine grain nucleation compared to that obtained in the case of higher thermal contact resistance (10^{-6} m^2 K/W).

It has been experimentally observed [6] that, on stainless steel substrates, a good thermal contact between the splat and the underlying surface can be obtained on surfaces exhibiting more peaks than undercuts. Such a surface topography is characterized by the skewness parameter $S_k > 0$, and favors the effective contact between the splat and the substrate. On the contrary, a poor thermal contact between the splat and substrate corresponds to a skewness parameter $S_k \leq 0$ and a lower cooling rate. The predicted mean grain radius is about 30 nm when the contact is nearly perfect (10^{-8} m^2 K/W) and about 150 nm when the quality of contact is poor (Fig. 7).

The cooling rate obtained for a low contact resistance is of the order of $5 \cdot 10^8$ K/s while it is about $2 \cdot 10^7$ K/s in the case of higher thermal contact resistance (10^{-6} m^2 K/W). Both values are close to those experimentally obtained by Bianchi et al. [4]

3.2.4. Effect of the oxide layer

Preheating metallic substrates over the transition temperature results in disk-shaped splats, but it also induces the growth of an oxide layer on the substrate surface. The effect of this layer on the crystal growth kinetics in an alumina splat has been taken into account by considering two types of steel: stainless steel 304 L and low carbon steel XC38 [25]. The oxide layer developed on stainless steel 304 L substrate was about 40-nm thick and its effect on the nucleation process was negligible while the oxide layer developed on low carbon steel was about 500 nm [19] and might affect the splat cooling and solidification processes.

Fig. 8 shows the effect of the oxide layer on the grain size distribution in an alumina splat deposited on low carbon steel substrate (XC38). The oxide layer, composed of Fe_2O_3 and Fe_3O_4, was included in the model taking into account the heat flux conservation at the interface lamella/oxide layer according to

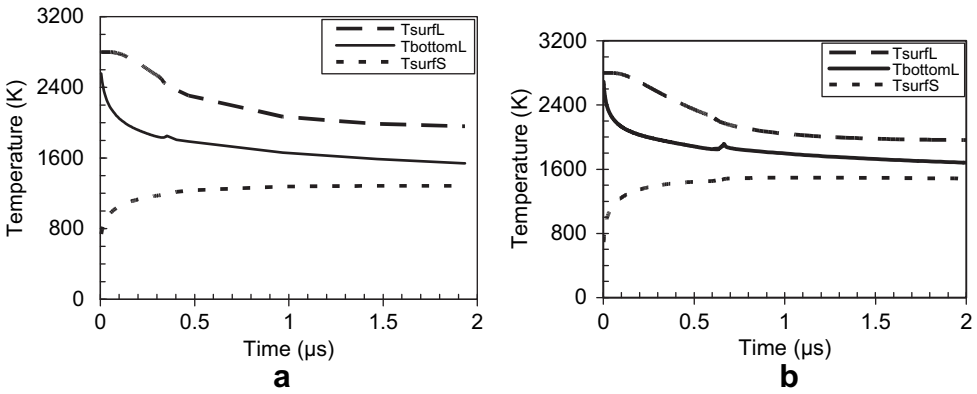

Fig. 5. Thermal history of alumina splat, 1-µm thick, $R_{th} = 10^{-7}$ m^2 K/W, deposited on: (a) stainless steel 304 L substrate, (b) γ-alumina substrate.

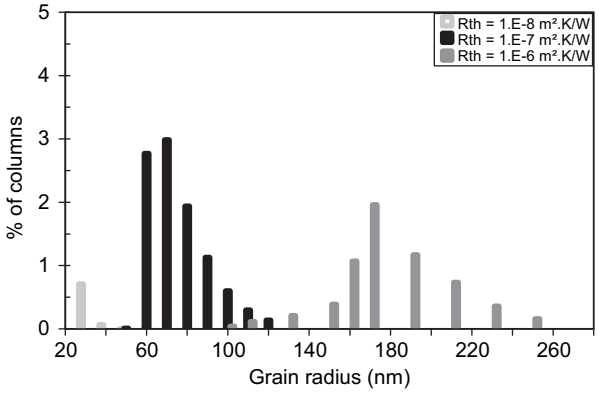

Fig. 7. Variation of the grain size distribution with the quality of the splat–substrate contact. Alumina splat 1-μm thick deposited on stainless steel substrate.

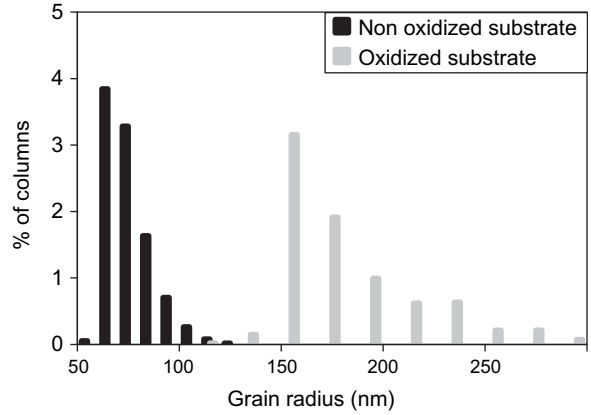

Fig. 8. Effect of the oxidation of a low carbon steel substrate on the grain size distribution in an alumina splat, 2-μm thick, $T_0 = 573$ K.

equation (4). We consider a perfect contact between the oxide layer and the substrate; this approach is described elsewhere [25]. This affects the heat release to the substrate and leads to the formation of larger grains. A grain mean radius on the order of 160 nm is obtained for an oxidized low carbon steel substrate to be compared to 65 nm for the same substrate in the absence of the oxide layer.

4. Experimental observations

The grain size determined from micrographies of plasma-sprayed alumina splats obtained by atomic force microscopy [4] (Fig. 9) are compared to the grain parameters calculated in this study. This comparison is summarized in Table 3 whose first column presents the nature of the used substrates that were all preheated at 573 K: stainless steel, gamma-alumina phase and alpha-alumina phase substrate. The phase of the alumina splats deposited on these substrates is gamma. Spraying was performed with a DC plasma torch working with Ar–H_2 gas mixture (45slm Ar–15slm H_2) and an anode-nozzle 7 mm in internal diameter. The molten particles whose size ranged between 22 and 45 μm, impacted onto the substrate with a velocity of about 250 m/s and a temperature of about 3400 K. The alumina splats collected on the preheated had a mean diameter of about 100 μm with a thickness of about 1.1 μm.

The grain radii and densities obtained from AFM observation of alumina splats deposited on stainless steel, gamma and alpha-alumina substrates, respectively, corresponded to the following contact angle: 78°, 70° and 75°, respectively. In order to compare the calculated and experimental grain parameters, the previous contact angles were used for the calculations and the resulting grain parameters were quite similar to the calculated ones.

In Table 3 are also reported a wide range of grain radii obtained experimentally for alumina splats deposited on stainless steel substrate (50–150 nm). AFM observations of alumina splats deposited on preheated stainless steel substrate showed the existence of two types of crystal shapes: big crystals with rather regular shape (columnar crystals of about 150 nm in radius) and small crystals of about 50 nm in radius [4]. These values correspond to a mean grain radius of the order of 55 nm in good agreement with the calculated value of 53 nm. This type of microstructure was explained by the presence of zones with various contact quality at the splat–substrate interface.

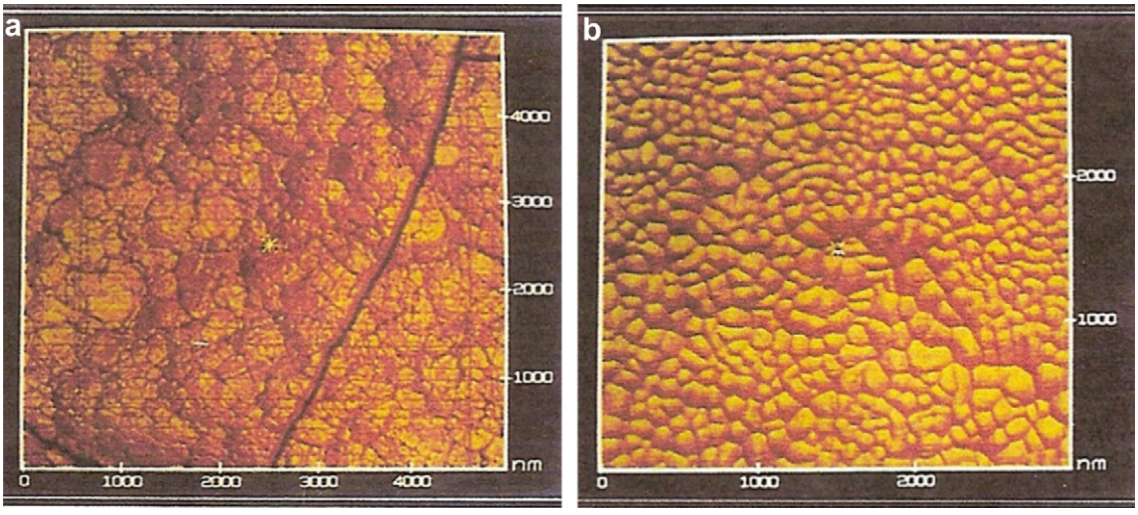

Fig. 9. AFM pictures of plasma-sprayed alumina splats deposited on: (a) stainless steel substrate (304 L), (b) γ-alumina substrate [4].

Table 3
Comparison of experimental and predicted grain parameters.

Substrate Preheated at 573 K	Experimental values		Calculated values			
	Grain density (μm^{-2})	Mean grain radius (nm)	Contact angle (°)	Grain density (μm^{-2})	Mean grain radius (nm)	Splat diameter (μm)
Stainless steel 304 L		50–150	**78**	65	53	85
γ-Al_2O_3	60	55	**70**	60.8	55	85
α-Al_2O_3	20	100	**75**	22	96	85

The results of Table 3 also suggest that the contact angle ranges between 70° and 80°.

5. Conclusion

In this study a one-dimensional heat transfer model taking into account the non-equilibrium solidification of alumina splats deposited onto metallic or ceramic substrates is presented. The model includes under-cooling phenomenon, heterogeneous nucleation at the substrate surface and crystal growth kinetics. It makes also possible to take into account an oxide layer at the substrate surface.

The numerical calculations show that the contact angle between the nucleus and the substrate surface as well as the quality of the contact at the splat–substrate interface, modelled by a thermal contact resistance R_{th}, are the two key parameters conditioning the nucleation temperature, grain size and density and, therefore, to a large extent the coating microstructure. The comparison of predicted and actual grain sizes (determined from AFM pictures of alumina splats deposited on stainless steel and alumina substrates) suggests that the contact angle ranges between 70° and 80°.

Experiments have shown that preheating the substrate improves the quality of contact at the splat–substrate interface. This results in an increase in splat cooling rate that can reach $5 \cdot 10^8$ K/s. A poor contact induces the formation of larger grain.

These predictions are in good agreement with the experiments: a grain mean radius of about 60 nm is predicted in the case of a good splat/substrate contact (corresponding to $R_{th,} = 10^{-7}$ m^2 K/W) whereas it is higher than 100 nm in the case of a poor contact ($R_{th,} = 10^{-6}$ m^2 K/W).

The effect of a 500-nm thick oxide layer, developed after preheating on a low carbon steel substrate surface, has also been investigated. Calculations show that the oxide layer affects the heat evacuation to the substrate leading to an increase in the grain mean radius.

References

[1] P. Fauchais, M. Fukumoto, A. Vardelle, M. Vardelle, Knowledge concerning splat formation: an invited review. J. Therm. Spray Technol. 13 (2004) 337–360.
[2] M. Fukumoto, E. Nishioka, T. Nishiyama, New criterion for splashing in flattening of thermal sprayed particles onto flat substrate surface. Surf. Coatings Technol. 161 (2002) 103–110.
[3] M. Fukumoto, M. Shiba, H. Haji, T. Yasui, Three-dimensional transition map of flattening behaviour in the thermal spray process. Pure Appl. Chem. 77 (2) (2005) 429–442.
[4] L. Bianchi, A.C. Leger, M. Vardelle, A. Vardelle, P. Fauchais, Splat formation and cooling of plasma-sprayed zirconia. Thin Solid Films 305 (1997) 35–47.
[5] C. Escure, M. Vardelle, P. Fauchais, Experimental and theoretical study of the impact of alumina droplet on cold and hot substrates. Plasma Chem. Plasma Process 3 (2003) 291–309.
[6] J. Cedelle, M. Vardelle, P. Fauchais, Influence of stainless steel substrate preheating on surface topography and on millimeter- and micrometer-sized splat formation. Surf. Coatings Technol. 201 (2006) 1373–1382.
[7] M. Bussmann, S.D. Aziz, S. Chandra, J. Mostaghimi, 3D modelling of thermal spray droplet splashing. in: C. Coddet (Ed.), Thermal Spray: Meeting the Challenges of the 21st Century. ASM International, Materials Park, 1998, pp. 413–418.
[8] R. Dhiman, A. McDonald, S. Chandra, Predicting splat morphology in a thermal spray process. Surf. Coatings Technol. 201 (18) (2007) 7789–7801.
[9] G. Trapaga, E.F. Mathys, J.J. Valencia, J. Szekely, Fluid flow, heat transfer and solidification of molten metal droplets impinging on substrates: comparison of numerical and experimental results. Metall. Trans. B 23 (1992) 701–718.
[10] J. Fukai, Z. Zhao, D. Poulikakos, C.M. Megaridis, O. Miyatake, Modeling of the deformation of a liquid droplet impinging upon a flat surface. Phys. Fluids A 5 (1993) 2588–2599.
[11] M. Bertagnolli, M. Marchese, G. Jacucci, I.St. Doltsinis, S. Noelting, Thermomechanical simulation of the splashing of ceramic droplets on a rigid substrate. J. Comput. Phys. 133 (1997) 205–221.
[12] M. Bussmann, J. Mostaghimi, S. Chandra, On a three-dimensional volume tracking model of droplets impact. Phys. Fluids 11 (1999) 1406–1417.
[13] M. Bussmann, S. Chandra, J. Mostaghimi, Modeling the splash of a droplet impacting a solid surface. Phys. Fluids 12 (2000) 3121–3132.
[14] D.B. Kothe, R.C. Mjolsness, M.D. Torrey, Technical Report, LA-12007-Ms, Los Alamos National Laboratory, 1991.
[15] M. Pasandideh-Fard, V. Pershin, S. Chandra, J. Mostaghimi, Splat shapes in a thermal spray coating process: simulations and experiments. J. Therm. Spray Technol. 11 (2) (2002) 206–217.
[16] X. Jiang, Y. Wan, H. Herman, S. Sampath, Role of condensates and adsorbates on substrate surface on fragmentation of impinging molten droplets during thermal spray. Thin Select Films 385 (1–2) (2001) 132–161.
[17] P. Fauchais, Understanding plasma spraying. J. Phys. D: Appl. Phys. 37 (2004) 86–108.
[18] L. Bianchi, A. Grimaud, F. Blein, P. Lucchese, P. Fauchais, Comparison of plasma sprayed alumina coatings by RF and DC plasma spraying. J. Thermal Spray Technol. 4 (1) (1995) 95–100.
[19] J. Pêch, Préoxydation générée par jet de plasma d'arc soufflé, relation entre surface d'oxydation et adhérence des dépôts. PhD thesis, University of Limoges, France, 1999.
[20] M. Vardelle, A. Vardelle, P. Fauchais, C. Moreau, Pyrometer system for monitoring the particle impact on a substrate during plasma spray process. Meas. Sci. Technol. 5 (1994) 205–213.
[21] H. Zhang, X.Y. Wang, L.L. Zheng, X.Y. Jiang, Studies of splat morphology and rapid solidification during thermal spraying. Int. J. Heat Mass Transfer 44 (2001) 4579–4592.
[22] C. Robert, A. Denoirjean, A. Vardelle, G.X. Wang, S. Sampath, Nucleation and phase selection in plasma-sprayed alumina: modeling and experiment. in: C. Coddet (Ed.), Thermal Spray: Meeting the Challenges of the 21st Century. ASM International, Materials Park, 1998, pp. 767–772.
[23] G.-X. Wang, V. Prasad, S. Sampath, H. Hermann, Modeling of Rapid Solidification During Splat Quenching Solidification. The Minerals, Metals & Materials Society/AIME, 1998, pp. 485–496.
[24] H. Zhang, X.Y. Wang, L.L. Zheng, S. Sampath, Numerical simulation of nucleation, solidification, and microstructure formation in thermal spraying. Int. J. Heat Mass Transfer 47 (2004) 2191–2203.
[25] Y. Mebdoua, Numerical Study of the Thermal Phenomena Controlling Splat Solidification Under Plasma Spray Conditions: Application to the Coating Construction, PhD thesis, University of Limoges, France, 2008.
[26] C.G. Levi, V. Jayaram, J.J. Valencia, R. Mehrabian, Phase selection in electrohydrodynamic atomization of alumina. J. Mater. Res. 3 (5) (1988) 969–983.
[27] Y. Lahmar, A. Vardelle, P. Fauchais, D. Gobin, Heat transfer and non-equilibrium phase change of lamellae under plasma spray conditions. J. High Temperature Mater. Process. 11 (2) (2007) 191–204.
[28] H.G. Landau, Heat conduction in a melting solid. Quart. Appl. Math. 8 (1) (1950) 81–94.
[29] N.J. Ruperti, D. Gobin, R.M. Cotta, Covalidation of integral transform and finite volume solutions in phase-change problems, in: 7th Latin-American Heat and Mass Transfer Conference – ENCIT 98 (Rio de Janeiro), 1998, pp. 659–664.
[30] A.C. Leger, M. Vardelle, A. Vardelle, P. Fauchais, S. Sampath, C.C. Berndt, H. Herman, Plasma sprayed zirconia: relationships between particles parameters, splat formation and deposit generation. Part I: impact and solidification. in: C.C. Berndt (Ed.), Thermal Spray: Practical Solutions for Engineering Problems. ASM International, Materials Park, 1996, pp. 623–628.
[31] R. Mc Pherson, On the formation of thermally sprayed alumina coatings. J. Mater. Sci. 25 (1980) 3677–3682.